The Journal of the Astronautical Sciences, Vol. 54, No. 1, January–March 2006, pp. 000–000

Nondimensional Star Identification for Uncalibrated Star Cameras[1]

Malak A. Samaan,[2] Daniele Mortari,[3] and John L. Junkins[4]

Abstract

Star identification is the most critical and important process for attitude estimation, given data from any star sensor. The main purpose of the Star Identification (Star-ID) process is to identify the observed/measured stars with the corresponding cataloged stars. The precision of the observed star directions highly depend on the calibrated accuracy of the star camera parameters, mainly the focal length f, and the optical axis offsets (x_0, y_0). When these parameters are not accurate or when the camera is not well calibrated, the proposed Nondimensional Star-ID method becomes very suitable, because it does not require accurate knowledge of these parameters. The Nondimensional Star-ID method represents a unique tool to identify the stars of uncalibrated or inaccurate parameters cameras. The basic idea derives the identification process from the observed focal plane angles which are, to first order, independent from both the focal length and the optical axis offsets. The adoption of the k-vector range search technique, makes this method very fast. Moreover, it is easy to implement, accurate, and the probability of failing Star-ID is less than 0.1% for typical star tracker design parameters.

Introduction

For successful Star-ID, some camera parameters such as effective focal length and optical axis offsets, should be carefully determined before used on any space mission. These parameters can be estimated in the laboratory or using a recently developed ground calibration algorithm (reference [1]). However, due to some in flight distortion of the focal plane, or some cyclic thermal deformations, these parameters may not remain accurate over the mission lifetime. Therefore, a method that can accomplish the Star-ID process for poorly calibrated cameras, or when

[1]Presented as paper AAS 03-131 at the 13th Annual AAS/AIAA Space Flight Mechanics Meeting, February 9–13, 2003, Ponce, Puerto Rico.
[2]Research Associate, National Authority for Remote Sensing and Space Sciences, Cairo, Egypt. Tel. +202 622-5821, samaan@gmail.com.
[3]Associate Professor, Department of Aerospace Engineering, Texas A&M University, College Station, Texas 77843-3141. Tel: (979) 845-0734, Fax: (979) 845-6051, mortari@tamu.edu.
[4]George J. Eppright Chair Professor, Director of the Center for Mechanics and Control, Department of Aerospace Engineering, Texas A&M University, College Station, TX 77843-3141. Tel: (979) 845-3912, Fax: (979) 845-6051, junkins@tamu.edu.

previous accurate camera parameters are not accurate for a camera undergoing environmental change, is required. Such a method is introduced in this paper as the *"Nondimensional Star-ID"* algorithm.

The *Nondimensional Star-ID* method is used herein to identify stars without *a priori* attitude information (Lost-In-Space). Several algorithms have been developed before to solve the Lost-In-Space Star-ID problem as in reference [2] and reference [3], but all these algorithms assume known values of the camera parameters, while in this paper we present a novel method that can solve the same problem with poorly calibrated or uncalibrated star cameras.

In particular, it is demonstrated that the relation between the angles of the cataloged triangles (α_i) and the corresponding angles of focal plane measured triangles (β_i) are independent, to the first order, of the camera basic parameters, (x_0, y_0) and f, which quantify the optical axis offsets and the camera focal length, respectively. Their differences will reflect primarily centroiding errors and, secondary, higher order distortions. For the typical case, usual manufacturing tolerance will result in these higher order distortions being sufficiently small that the Nondimensional Star-ID method is very reliable. Moreover, it is possible to demonstrate that, on a first approximation, the angles of focal plane triangles are also independent of the rotation. The fact that variations in (x_0, y_0, f) simply shift and scale the triangles (to first-order), means that using in-plane angles for Star-ID can likely be done with very poor estimates of (x_0, y_0, f). Figure 1 shows two star images for different focal lengths, and optical axis offsets.

To validate our proposed Nondimensional Star-ID method, both night-sky tests and Monte Carlo simulations have been used to quantify its performances.

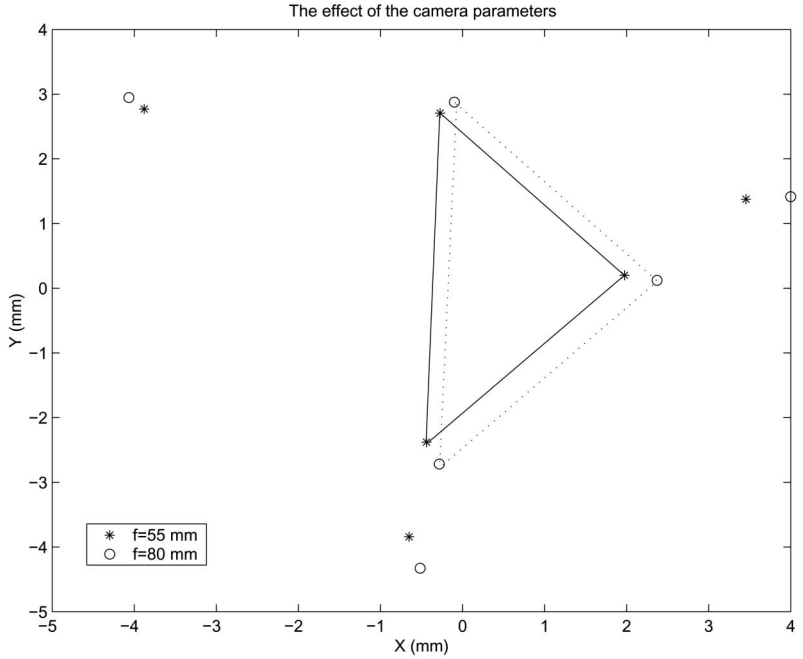

FIG. 1. Star Image for Two Different Focal Lengths.

Also, the Nondimensional Star-ID algorithm can be used as the first step for the focal plane calibration to find camera basic parameters without any need to identify the stars by sight.

Focal Plane and Inertial Angles

Assuming that the star tracker can be modelled as an ideal pin-hole camera (see Fig. 2), the body vector ($\mathbf{b}_i$) of any star measurement is related to the corresponding inertial unit-vector $\hat{\mathbf{r}}_i$ through

$$\mathbf{b}_i = \begin{Bmatrix} -(x_i - x_0) \\ -(y_i - y_0) \\ f \end{Bmatrix} = m_i \, \hat{\mathbf{b}}_i = m_i \, C \, \hat{\mathbf{r}}_i \tag{1}$$

where C is the attitude matrix, $m_i = \sqrt{(x_i - x_0)^2 + (y_i - y_0)^2 + f^2}$, f is the focal length, and (x_0, y_0) are the optical axis offsets. Equation (1) allows us to write

$$\begin{cases} \Delta\mathbf{b}_{ij} = \mathbf{b}_j - \mathbf{b}_i = \begin{Bmatrix} x_i - x_j \\ y_i - y_j \\ 0 \end{Bmatrix} = C(m_j\hat{\mathbf{r}}_j - m_i\hat{\mathbf{r}}_i) \\ \Delta\mathbf{b}_{ik} = \mathbf{b}_k - \mathbf{b}_i = \begin{Bmatrix} x_i - x_k \\ y_i - y_k \\ 0 \end{Bmatrix} = C(m_k\hat{\mathbf{r}}_k - m_i\hat{\mathbf{r}}_i) \end{cases} \tag{2}$$

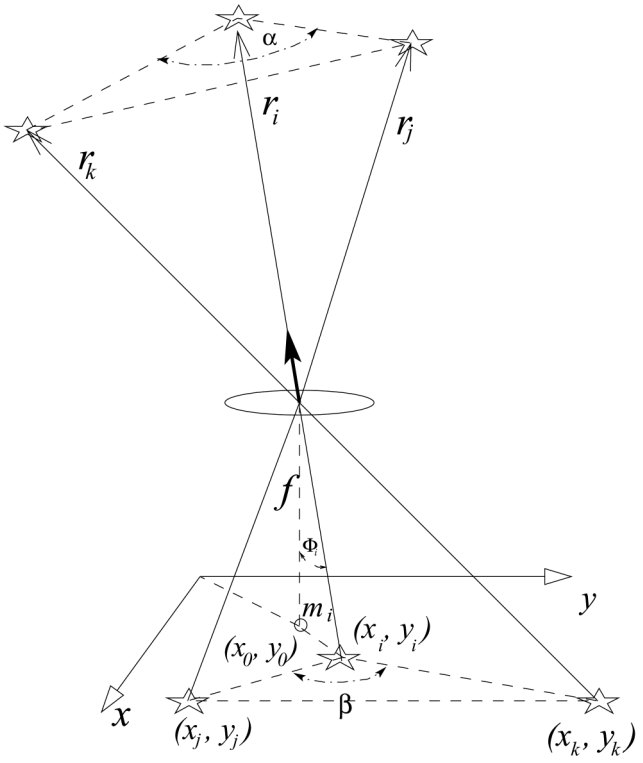

FIG. 2. Geometry for a Pin-Hole Camera (Colinearity Condition).

Let us introduce the angle α (see Fig. 2) as the angle between the two reference vectors $\Delta\mathbf{r}_{ij} = \hat{\mathbf{r}}_j - \hat{\mathbf{r}}_i$ and $\Delta\mathbf{r}_{ik} = \hat{\mathbf{r}}_k - \hat{\mathbf{r}}_i$, as

$$\cos\alpha = \frac{(\Delta\mathbf{r}_{ij})^{\mathrm{T}}(\Delta\mathbf{r}_{ik})}{\|\Delta\mathbf{r}_{ij}\|\|\Delta\mathbf{r}_{ik}\|} \tag{3}$$

Also, assuming the usual pin-hole camera model, the corresponding focal plane angle (β) is evaluated as

$$\cos\beta = \frac{(\Delta\mathbf{b}_{ij})^{\mathrm{T}}(\Delta\mathbf{b}_{ik})}{\|\Delta\mathbf{b}_{ij}\|\|\Delta\mathbf{b}_{ik}\|} = \frac{(x_j - x_i)(x_k - x_i) + (y_j - y_i)(y_k - y_i)}{\sqrt{(x_j - x_i)^2 + (y_j - y_i)^2}\sqrt{(x_k - x_i)^2 + (y_k - y_i)^2}} \tag{4}$$

Since, for typical star tracker cameras, f^2 is usually much greater than $(x_i - x_0)^2 + (y_i - y_0)^2$, then the vector modulus m_i is just a little bit greater than f. Therefore, the vector modulus m_i may be expressed as

$$m_i = f(1 + \delta_i) \qquad \Leftrightarrow \qquad \delta_i = \frac{m_i - f}{f} \tag{5}$$

where $i = j, k$. Let ϕ_i be the angle between the i-th observed direction $\mathbf{b}_i$ and the camera optical axis. Then, for a 10° pin-hole camera ~~(max~~ ($\max \phi_i = 5°$, $\cos\phi_i \cong 0.9962$ and $f = m_i\cos\phi_i$), we have the upper limit $\delta_i = (\cos\phi_i)^{-1} - 1 < 0.0038$. Therefore, equation (2) becomes

$$\begin{cases} \Delta\mathbf{b}_{ij} = fC[(1 + \delta_j)\hat{\mathbf{r}}_j - (1 + \delta_i)\hat{\mathbf{r}}_i] = fC[\hat{\mathbf{r}}_j - \hat{\mathbf{r}}_i + \delta_j\hat{\mathbf{r}}_j - \delta_i\hat{\mathbf{r}}_i] \\ \Delta\mathbf{b}_{ik} = fC[(1 + \delta_k)\hat{\mathbf{r}}_k - (1 + \delta_i)\hat{\mathbf{r}}_i] = fC[\hat{\mathbf{r}}_k - \hat{\mathbf{r}}_i + \delta_k\hat{\mathbf{r}}_k - \delta_i\hat{\mathbf{r}}_i] \end{cases} \tag{6}$$

We can notice the last two terms in equation (6) are small <0.0038. Substituting equation (6) into equation (4), and using $C^{\mathrm{T}}C = I$, we obtain

$$\cos\beta = \frac{(\mathbf{r}_j - \mathbf{r}_i)^{\mathrm{T}}(\mathbf{r}_k - \mathbf{r}_i) + N + \varepsilon}{D_1 D_2} \tag{7}$$

where

$$\begin{cases} N = \delta_j\mathbf{r}_j^{\mathrm{T}}(\mathbf{r}_k - \mathbf{r}_i) - \delta_i\mathbf{r}_i^{\mathrm{T}}(\mathbf{r}_k - \mathbf{r}_i) + \delta_k\mathbf{r}_k^{\mathrm{T}}(\mathbf{r}_j - \mathbf{r}_i) - \delta_i\mathbf{r}_i^{\mathrm{T}}(\mathbf{r}_j - \mathbf{r}_i) \\ D_1 = \sqrt{(\mathbf{r}_j - \mathbf{r}_i)^{\mathrm{T}}(\mathbf{r}_j - \mathbf{r}_i) + 2(\delta_j\mathbf{r}_j - \delta_i\mathbf{r}_i)^{\mathrm{T}}(\mathbf{r}_j - \mathbf{r}_i)} \\ D_2 = \sqrt{(\mathbf{r}_k - \mathbf{r}_i)^{\mathrm{T}}(\mathbf{r}_k - \mathbf{r}_i) + 2(\delta_k\mathbf{r}_k - \delta_i\mathbf{r}_i)^{\mathrm{T}}(\mathbf{r}_k - \mathbf{r}_i)} \\ \varepsilon = \delta_j\delta_k\mathbf{r}_j^{\mathrm{T}}\mathbf{r}_k - \delta_j\delta_i\mathbf{r}_i^{\mathrm{T}}\mathbf{r}_j - \delta_i\delta_k\mathbf{r}_i^{\mathrm{T}}\mathbf{r}_k + \delta_i^2 \end{cases} \tag{8}$$

For negligible (δ_i, δ_j, δ_k), equation (7) will be identical to equation (3), and then $\beta = \alpha$. Notice that $\cos\beta$ depends on (x_0, y_0, f) only through the small (δ_i, δ_j, δ_k) terms. Since the δ_i terms are of order ~ 0.0038, small errors in (x_0, y_0, f) perturb small terms, making sensitivity with respect to (x_0, y_0, f) errors low. For example, the δ_i variation due to Δf error, can be written as

$$\begin{aligned} \Delta\delta_i &= \frac{\partial\delta_i}{\partial f}\Delta f + h.o.t. = \left(\frac{\frac{\partial m_i}{\partial f} - 1}{f} - \frac{m_i - f}{f^2}\right)\Delta f + h.o.t. \\ &= \left(\frac{\frac{1}{\cos\phi_i} - \frac{m_i}{f}}{f}\right)\Delta f + h.o.t. \end{aligned} \tag{9}$$

The first order approximation of equation (9) for the $\hat{d}_i$ variation due to Δf error is equal to zero, but the higher order approximation create small errors of δ_i variation due to Δf. As typical example, if $f = 60$ mm and $\Delta f = 30$ mm (which is very large error in focal length!), we obtain $\Delta\delta_i < 10^{-4}$. For a more reasonable 1 mm error in f, we find $\Delta\delta_i < 10^{-6}$, which is smaller than typical centroiding errors of modern star trackers.

So, the worst case variation in $\hat{d}_i$ is at least one order of magnitude smaller than $\hat{d}_i$. This indicates that cos β has low sensitivity to any reasonable errors in f. This error in the cos β is typically lower than the tolerance (associated with camera accuracy) for our search. Even when we ignore δ_i corrections, we can achieve reliable Star-ID by considering redundant measured stars, as shown in the next section.

The Nondimensional Star-ID

The angles of a given catalog star triangle are evaluated as

$$\cos\alpha_1 = \frac{\mathbf{r}_{ij}^{\mathrm{T}}\mathbf{r}_{ik}}{\|\mathbf{r}_{ij}\|\|\mathbf{r}_{ik}\|}, \qquad \cos\alpha_2 = \frac{-\mathbf{r}_{jk}^{\mathrm{T}}\mathbf{r}_{ij}}{\|\mathbf{r}_{jk}\|\|\mathbf{r}_{ij}\|}, \qquad \cos\alpha_3 = \frac{\mathbf{r}_{ik}^{\mathrm{T}}\mathbf{r}_{jk}}{\|\mathbf{r}_{ik}\|\|\mathbf{r}_{jk}\|} \tag{10}$$

where $\mathbf{r}_{ij} = \mathbf{r}_j - \mathbf{r}_i$, $\mathbf{r}_{ik} = \mathbf{r}_k - \mathbf{r}_i$, and $\mathbf{r}_{kj} = \mathbf{r}_j - \mathbf{r}_k$.

The indices i, j, and k are chosen such that the minimum angle of the triangle (α_3) is always at vertex k. The indices of the cataloged vectors and the maximum and minimum angles of the focal plane triangles are stored in a matrix. Table 1 shows a portion of this star triangle data matrix sorted in ascending order of minimum angle (α_3).

The reference star catalog is obtained, in this paper, from Smithsonian Astrophysical Observatory (SAO) data in Epoch 2000 reference frame. The size of this matrix depends on the magnitude threshold. For instance, for a magnitude threshold of $M_{th} = 5.0$ and a $8^\circ \times 8^\circ$ Field-Of-View (FOV), the number of admissible triangles is 55,309, while for $M_{th} = 5.5$ and the same FOV size, the number of admissible triangles becomes 338,369.

TABLE 1. A Portion of the Star Triangle Data

k	I_1	I_2	I_3	α_1	α_3
11453	3903	1187	2230	102.1256	6.022182
11454	2434	725	2187	143.2689	6.022355
11455	729	3787	4722	101.0456	6.022963
11456	3487	1291	2229	130.1984	6.023178
11457	2128	3315	2641	147.359	6.023315
11458	483	2578	1424	147.5892	6.023319
11459	781	2895	3232	139.8646	6.023402
11460	4723	514	4195	141.9004	6.023447
11461	1315	667	3047	146.2288	6.023514
11462	632	2737	4757	118.9169	6.023539
11463	3684	1542	503	146.5031	6.023613

Figure 3 shows a plot of the smallest angle (α_3) versus the focal plane triangle index (k). In particular, no prior knowledge of (x_0, y_0, f) has been assumed, and the δ_i and δ_i^2 corrections in equation (10) have been ignored. We adopt a worst case tolerance for angle matching of 0.005 rad corresponding to the maximum δ_i possible over FOV.

Let us divide the smallest angle (α_3) into very small and uniform intervals of step size ($\delta\alpha_3$), and let us interpolate the value of (k) at any value of ($0° < \alpha_3 < 60°$). So, for ($\delta\alpha_3 = 0.001°$) we can store the values of α_3 and the corresponding index value k. Figure 4 illustrates this idea. Even though Fig. 3 looks smooth, there are evident fine structure variations on the finer scale of Fig. 4. The uniform in (α_3) table, a portion of which plotted in Fig. 4 is introduced to permit ultra high speed, search-less interpolation of the index k as a function of measured values of α_3.

Now, once we have the coordinates of any star image (x_i, y_i) we can find the focal plane angles established by any three stars. A catalog database of star triangles, sorted using the smallest angle of each triangle, is build and the k-vector range searching technique (see reference [7] for a complete description) is used to access it and obtaining the index range (from k_l to k_u) associated with the measured angle α_3 and its precision α_{3error}

$$k_l = \text{floor}\left(\frac{\alpha_3 - \alpha_{3error}}{\delta\alpha_3}\right) \quad \text{and} \quad k_u = \text{ceil}\left(\frac{\alpha_3 + \alpha_{3error}}{\delta\alpha_3}\right) \tag{11}$$

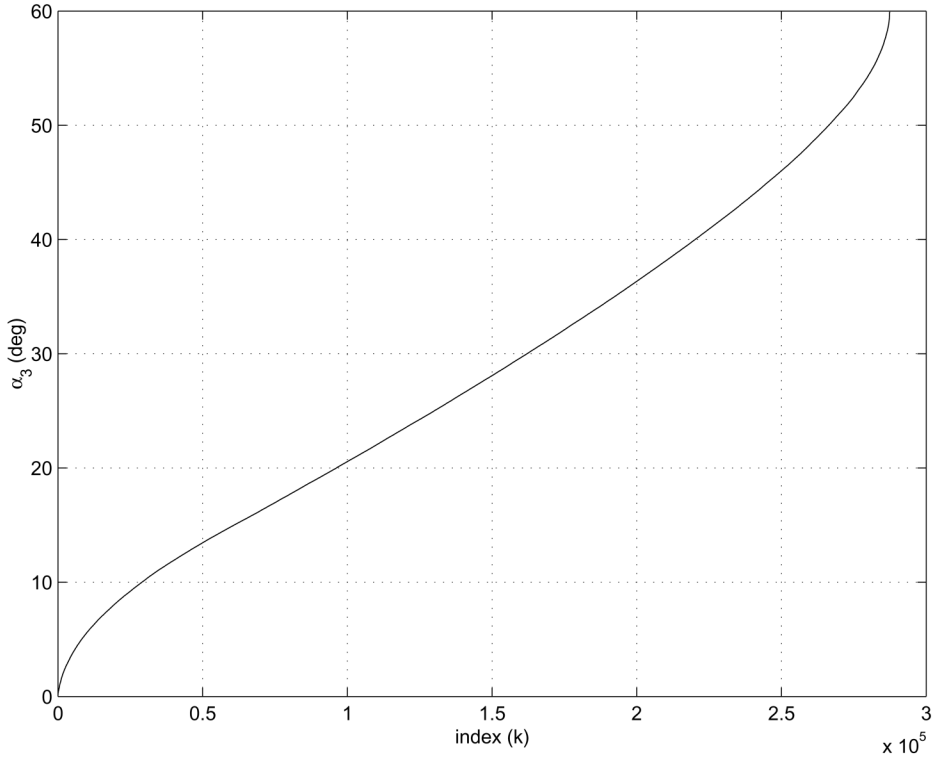

FIG. 3. The Smallest Focal Plane Angle Versus its Index.

using this range and by accessing the stored matrix for the cataloged indices we can find the range of the candidate triangles. By checking the largest angle α_1 we can find exactly which triangle in the catalog corresponds to the measured angle. As mentioned before, the worst case variation in δ_i is at least one order of magnitude smaller than δ_i, so we use a tolerance of $\alpha_{3error} = 500$ μ-rad corresponding to the maximum error in using equation (10) to approximate equation (7). Monte Carlo tests indicate occasional failures for three-star patterns, but negligible failures for five-star patterns (for 1,000 simulations no failures have been encountered).

Table 1 contains entries: k, $\alpha_3(k)$, $\alpha_1(k)$, $I_1(k)$, $I_2(k)$, $I_3(k)$, where $I_i(k)$ are the three-stars indices for the k-th cataloged triangle. The master catalog contains entries I, $M_v(I)$, $\lambda(I)$, $\mu(I)$, where I is the Star-ID integer, $M_v(I)$ is the visual magnitude, $\lambda(I)$ is the right ascension and $\mu(I)$ is the declination. If more than one triangle is found this triad of stars is skipped, and another triangle with different stars is formed until a unique matched triangle is found. If a unique triangle is found, which occurs in most cases, the Star-ID is then confirmed to high confidence using 4*th* and 5*th* stars to form new triangles sharing two stars with the first matched triangle. The rule is that all the inter-star angles of the polygon must match to within a given tolerance. Specifically, there are $\frac{n(n-1)}{2}$ angles for an n-star polygon. For the additional triangles the indices of the two common stars must also match. If this match fails, then the initial triangle match is rejected. The complete successful match represents the most common case, since the frequency of mismatch of four stars since, for a 5.5 magnitude threshold, $8^\circ \times 8^\circ$ FOV, and 512×512 CCD format, is on the order of 10^{-11}.

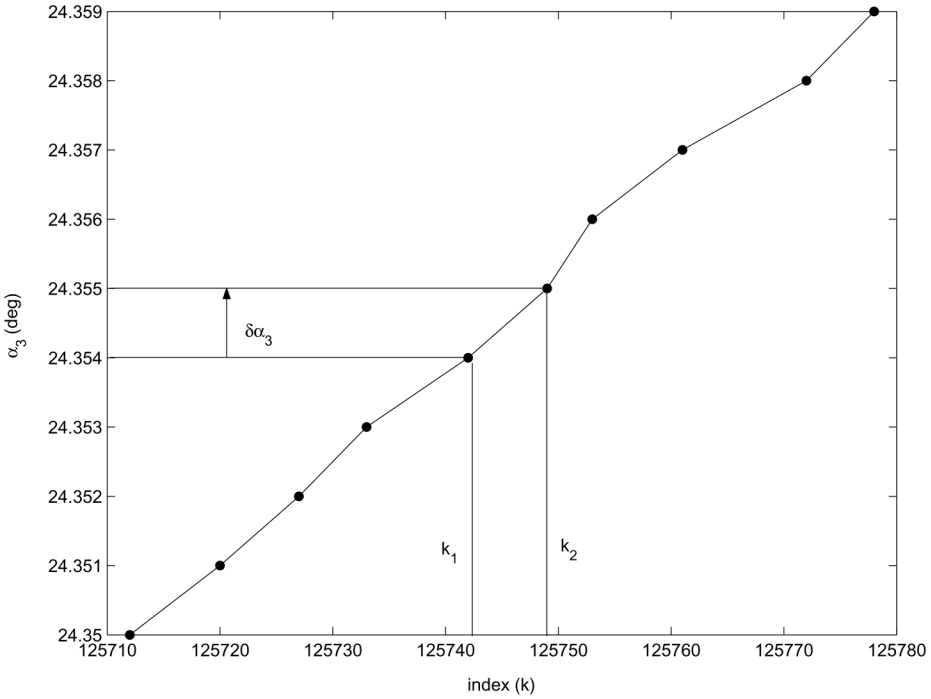

FIG. 4. α_3 Versus its Index.

Nondimensional Star-ID Algorithm Results

The proposed method has been successfully validated by both night-sky tests and Monte-Carlo simulations.

Using Night-Sky Tests

Repeated night-sky tests have been performed using the StarNav I prototype camera, the Pegasus 512×512 (reference [4]). Figure 5 shows an actual star image centered near $\lambda = 92°$, $\mu = 31°$. Figure 6 shows the coordinates of the star image evaluated by the centroiding algorithm (reference [5]).

Using the Nondimensional Star-ID algorithm we obtained the Star-ID results shown in Table 2. This table lists, for each identified star, the star identification number in the star catalog and the star right ascension and declination in the Earth Centered Inertial (ECI) reference frame.

Figure 7 shows the results obtained by the least square algorithm (see reference [1]) in estimating the optical axis offsets and the focal length. The least

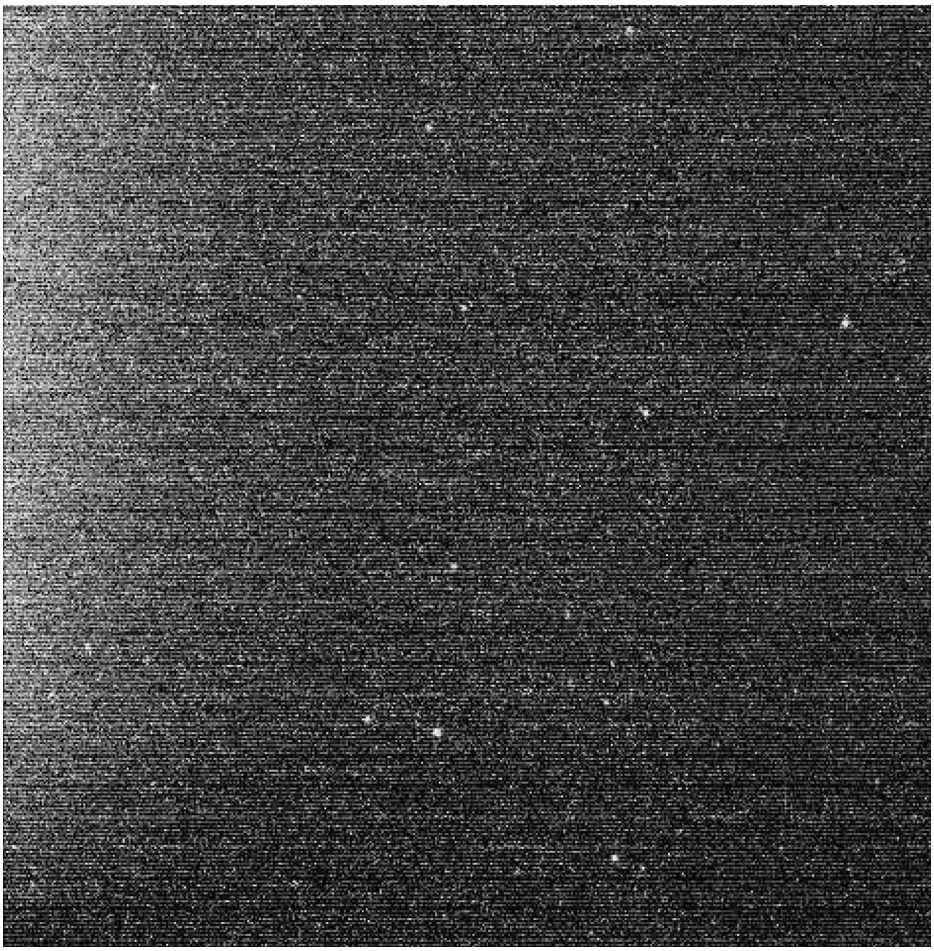

FIG. 5. Night-Sky Image Using Pegasus Camera.

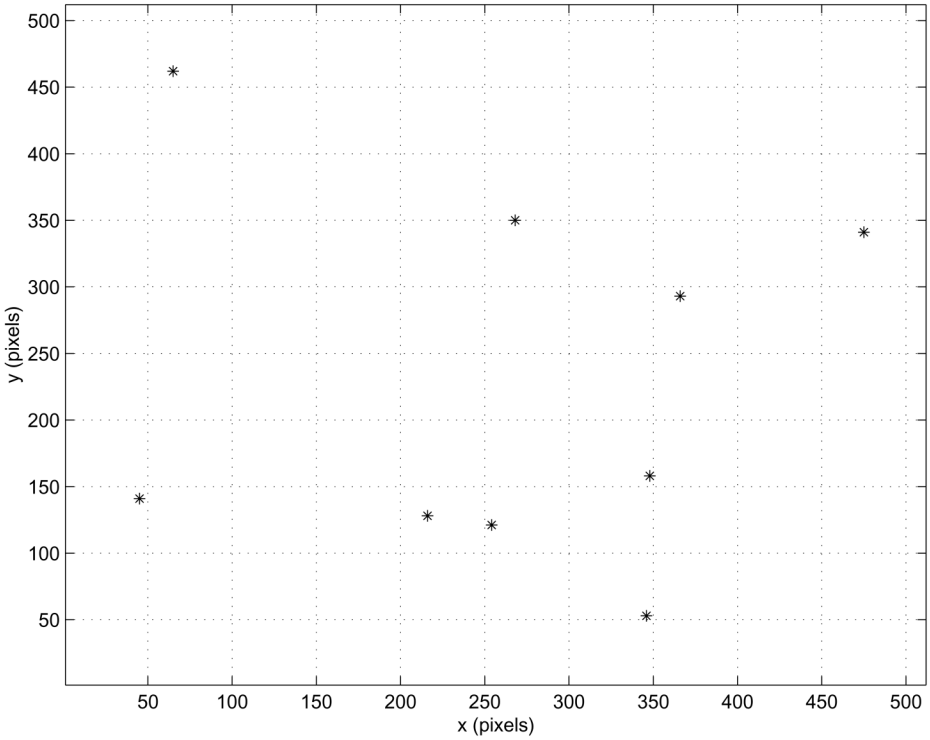

FIG. 6. Centroiding Results for the Pegasus Picture.

squares estimate provides us with the calibrated focal length $f_c = 52.3292$ mm, the calibrated $\hat{y}$-axis offset $x_0 = -0.28053$ mm, and the calibrated $\hat{x}$-axis offset $y_0 = -0.20124$ mm.

Moreover, using Fill-factory Star1000 (1024×1024 pixels) focal plane detector (see reference [8]), we developed a prototype star camera (StarNav II) for the Geosynchronous Imaging Fourier Transform Spectometer mission. In addition of simulations, night-sky tests, have been performed. Figure 8 shows a night-sky picture taken by the Star1000 camera.

Figure 9 shows the nine star coordinates (of the picture taken by the Star1000 Camera) obtained by the centroiding algorithm (reference [5]). The Star-ID results, obtained with the Nondimensional Star-ID Algorithm, are shown in Table 3. These results, combined with visual confirmation of the correct star identifications, validate the autonomous star identification process.

TABLE 2. Star-ID Results

Star-ID	669	1655	2546	1825	2545	2019
R.A. (deg)	−86.1554	−91.6681	−90.5015	−88.4066	−92.2581	−91.8330
Dec. (deg)	29.4983	27.6122	25.9538	29.5125	27.9679	33.9175

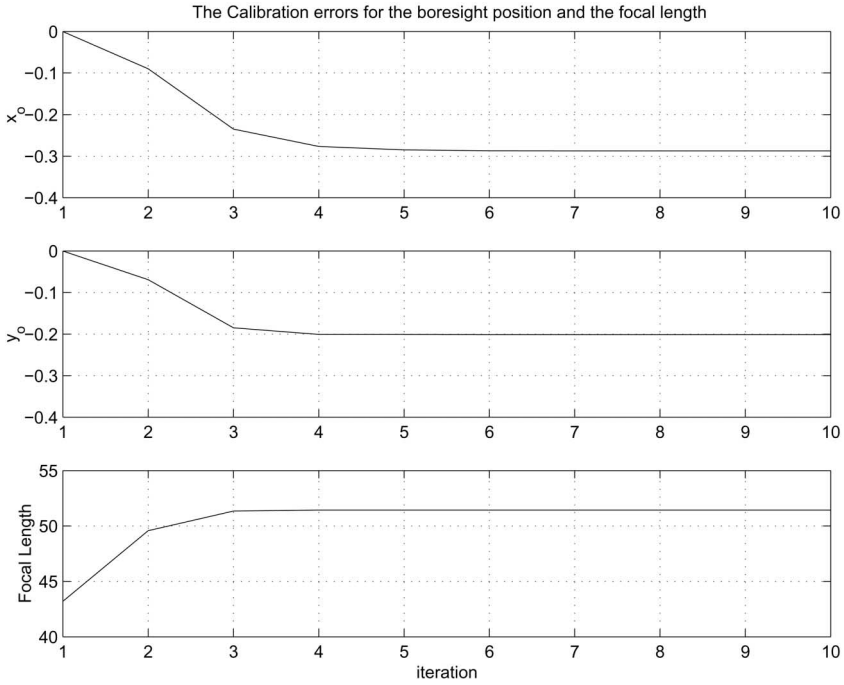

FIG. 7. Estimated Focal Length and Optical Axis Offsets.

FIG. 8. Night-Sky Image Using the Star1000 Camera.

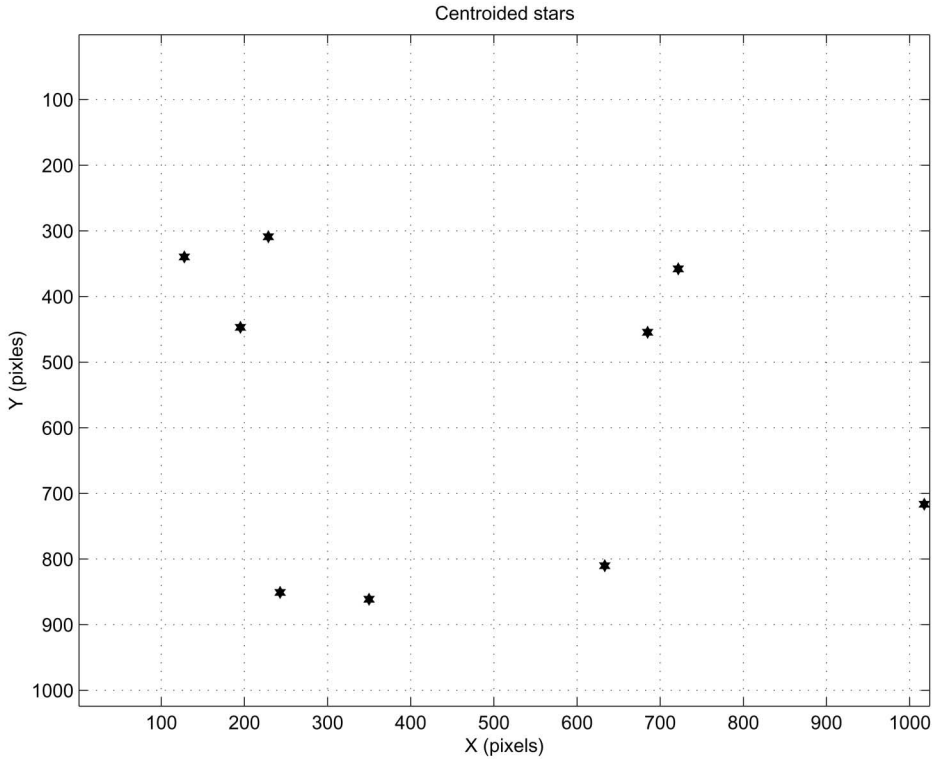

FIG. 9. Centroiding Results for the Star1000 Picture.

Using Monte-Carlo Simulations

Numerical simulations have been performed to verify the above results. We executed 1,000 tests using random spacecraft attitudes, while simulating star images with Gaussian centroiding errors. The resulting histogram of the number of observed star occurrences is shown in Fig. 10, while Fig. 11 provides the overall time required to perform the Nondimensional Star-ID (in seconds).

The performed 1,000 tests were 100% successful in accomplishing valid Star-ID, the actual expected success probability is believed to be well over 99%, based on approximations using a uniform star angular displacement density assumption. The failures occurred with scenarios involving too few valid imaged stars to form a triangle, or with scenarios involving approximate alignment of observed stars. In particular the latter case occurred with a probability less than 0.1%. These results highly depend on integration time and on the catalog construction. An alternative

TABLE 3. Star-ID Results for the Star1000 Image

Star-ID	1251	1255	945	936	1250	947	940	1249	1257
R.A. (deg)	42.537	50.129	49.729	56.125	42.021	44.812	45.673	40.904	50.595
Dec. (deg)	27.274	29.060	34.234	35.073	29.26	32.298	35.196	27.436	27.72

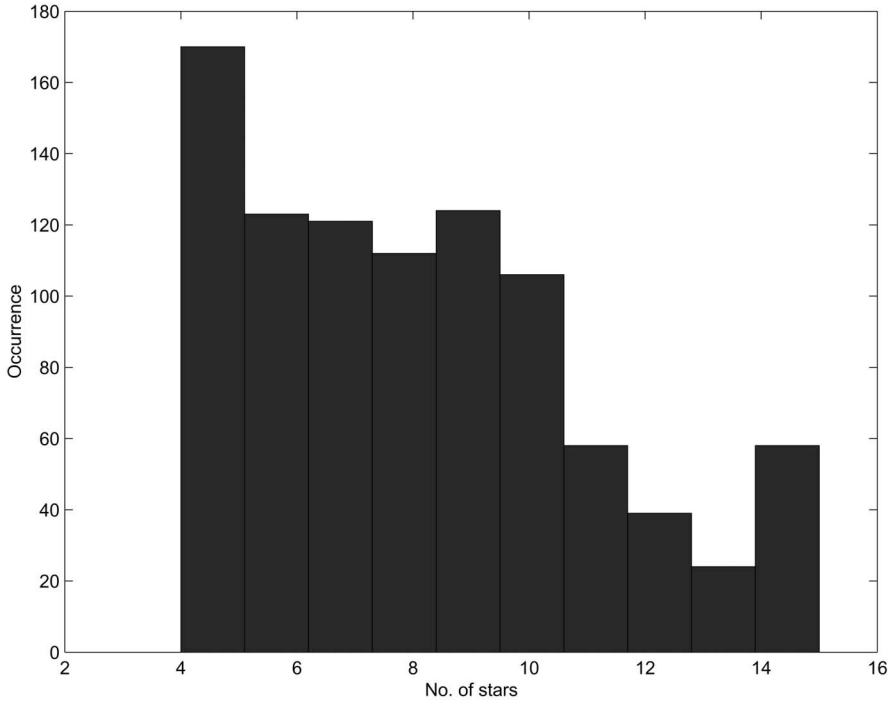

FIG. 10. Histogram of the Observed Number of Stars.

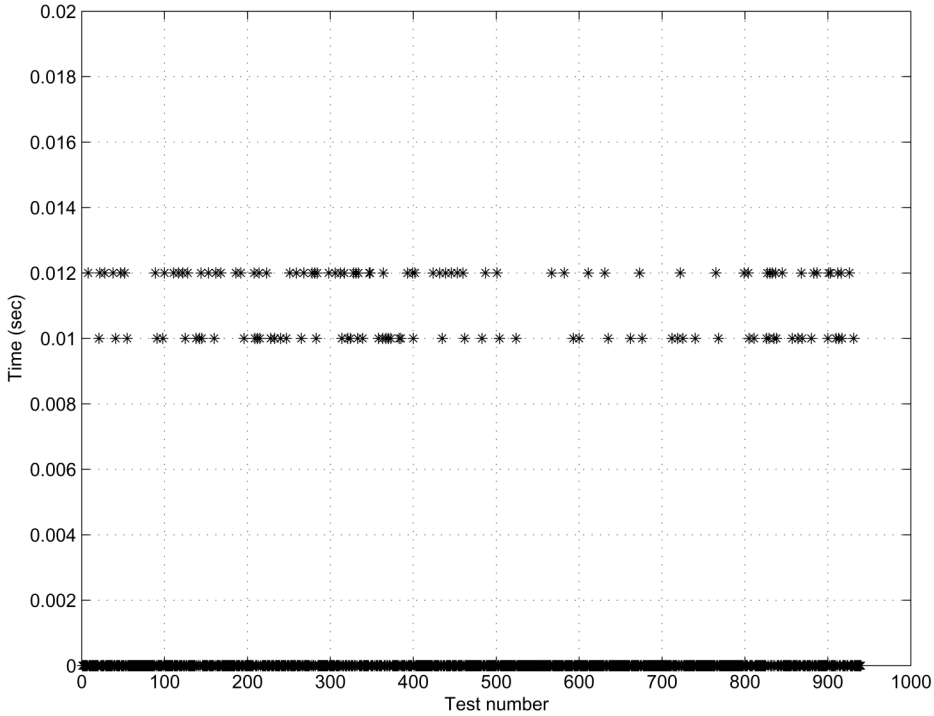

FIG. 11. Test Execution Times (in Seconds).

approach can be easily developed to take into account the small number of these special cases. For attitude estimation using rate gyro data, an occasional "drop out" due to sparse star fields, is well tolerated because typical rate gyros can be integrated for several minutes without appreciable accuracy degradation, while frame rates of star cameras are several frames per second.

The execution times given in Fig. 11 are obtained using a 600 Mhz Pentium III PC. These times, obviously, will be reduced with a better code implementation, but nonetheless, they provide a basis for our optimism as regards optimized flight codes. Other *k*-vector based Star-ID Algorithms, such as the more robust *Pyramid* Algorithm (see references [3], [6]), are dramatically faster. However, these faster algorithms require a well-calibrated camera, that is, an accurate knowledge of the focal length and of the optical axis offsets. It is clear that once the first Star-ID has been performed, the camera can be then calibrated using the method presented in reference [1], and, consequently, the *Pyramid* algorithm can be adopted to proceed with a robust and fast Star-ID process.

Analytical Estimation of the Focal Length

Once the observed stars have been identified, it is possible to estimate the focal length by the following procedure. As already mentioned, this is an important task, needed to initiate faster Star-ID algorithms as, for instance, the *Pyramid* algorithm. The procedure to estimate f, is summarized as follows.

1. From equation (1), if we assume (x_0, y_0) are negligible with respect to f, then we can write the interstar angle of the measured stars as

$$\cos\theta_{ij} = \mathbf{b}_i^{\mathrm{T}}\mathbf{b}_j = \frac{x_i x_j + y_i y_j + f^2}{\sqrt{x_i^2 + y_i^2 + f^2}\sqrt{x_j^2 + y_j^2 + f^2}} \tag{12}$$

   Note the difference between this equation, which calculates the interstar angle θ_{ij}, and equation (4) which calculates the focal plane angle.
2. The measured cosines should ideally equal the cataloged cosines $\cos\theta_{ij}$ which are, in turn, well known from dot product of cataloged vectors. Thus, the following equation contains just one unknown: the focal length f.

$$\cos^2\theta_{ij}[(x_i^2 + y_i^2 + f^2)(x_j^2 + y_j^2 + f^2)] = (x_i x_j + y_i y_j + f^2)^2 \tag{13}$$

3. By re-arranging equation (13) to the quadratic polynomial, then the roots of this polynomial represent the possible solutions for f

$$f^2 = \frac{(a+b)d^2 - 2c \pm \sqrt{[(a+b)d^2 - 2c]^2 - 4(1-d^2)(c^2 - abd^2)}}{2(1-d^2)} \tag{14}$$

   where $a = x_i^2 + y_i^2$, $b = x_j^2 + y_j^2$, $c = x_i x_j + y_i y_j$, and $d = \cos\theta_{ij}$.
4. Let us check the sign of $(c^2 - abd^2)$. For small FOV ($d^2 \cong 1$) we have

$$\begin{aligned} c^2 - abd^2 &= (x_i x_j + y_i y_j)^2 - (x_i^2 + y_i^2)(x_j^2 + y_j^2) \\ &\cong -[x_i^2 y_j^2 + y_i^2 x_j^2 - 2x_i x_j y_i y_j] \cong -[x_i y_j - x_j y_i]^2 \le 0 \end{aligned}$$

5. Since the sign of $[4(1-d^2)(c^2 - abd^2)]$ is negative, then the value of the square root will be greater than $[(a+b)d^2 - 2c]$. By choosing the positive sign of the square root (because f^2 must be positive), then we obtain an algebraic solution for f.

With this solution, the focal length with any star pair, can be estimated, and an improved average value of the focal length is obtained if more known stars are available.

The above analytical procedure has been tested using night-sky images, and simulated images. Both have been found to provide accurate estimates for the focal lengths.

This procedure assumed that the optical axis offsets (x_0, y_0) are negligible. However, this analytical solution has been validated with large specified optical axis offsets, such as $x_0 = -0.2$ mm, and $y_0 = 0.25$ mm, because we assume a small FOV where the offset values are one order of magnitude less than the focal length. Table 4 shows the star coordinates (in mm) and the Star-ID results obtained with a random attitude and a known camera focal length of $f = 55$ mm. The focal length has been evaluated using equation (14) for each star pair. Figure 12 plots the results obtained for f, for each star pair. The mean value of the focal length is found to be 55.0029 mm and the standard deviation is 0.0171. These results validate the assumption that the focal length is relatively insensitive to the (x_0, y_0) errors.

The approximate estimation of f obtained using equation (14), along with starting estimates of $(x_0 \simeq 0, y_0 \simeq 0)$ have been found to be good enough to ensure convergence of the nonlinear least squares algorithm (given in reference [1]), as a tool to obtain the final calibration estimates (x_0, y_0, f).

Error Variance Analysis

It is easy to show, for the typical values of focal plane dimensions and focal lengths, as those used to generate Fig. 1, that in equation (14) the term $4(1 - d^2)(c^2 - abd^2)$ is much smaller than the term $[(a + b)d^2 - 2c]^2$. By disregarding the second term an approximate solution for f

$$f \approx \sqrt{\frac{(a + b)d^2 - 2c}{1 - d^2}} \tag{15}$$

is obtained. Although equation (15) is not directly useful because it is only an approximation it is useful to help derive a simple variance of the error. A typical measurement model of star cameras considers the measurement errors of x_i, x_j, y_i, and y_j, be independent and white-noise Gaussian with equal variance, given by σ^2. Under these assumptions, a first-order approximation of the variance of the error in f is given by first computing the following partials

$$\frac{\partial f}{\partial x_i} = \frac{1}{\sqrt{\xi}}(x_i\, d^2 - x_j) \tag{16}$$

$$\frac{\partial f}{\partial x_j} = \frac{1}{\sqrt{\xi}}(x_j\, d^2 - x_i) \tag{17}$$

TABLE 4. Star Data for Random Attitude

X	2.2264	1.6275	2.5752	2.821	−0.305	1.8155	−1.9219	0.2891
Y	0.8718	2.0876	3.4253	2.195	3.3359	0.5425	−2.6363	−3.095
ID	408	677	678	1216	1331	1675	2304	2583

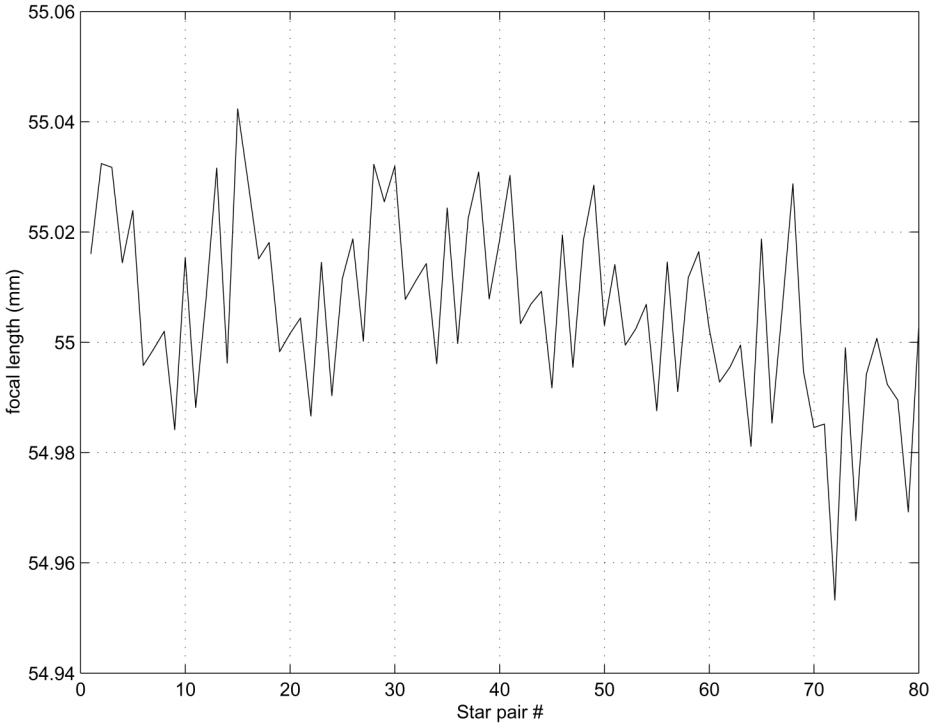

FIG. 12. Focal Length Estimation Results (for each Star Pair).

$$\frac{\partial f}{\partial y_i} = \frac{1}{\sqrt{\xi}}(y_i\, d^2 - y_j) \tag{18}$$

$$\frac{\partial f}{\partial y_j} = \frac{1}{\sqrt{\xi}}(y_j\, d^2 - y_i) \tag{19}$$

where

$$\xi = (1 - d^2)[(a + b)d^2 - 2c] \tag{20}$$

The variance of the error in f, denoted by σ_f^2, can be computed using

$$\sigma_f^2 = \sigma^2\, H^{\mathrm{T}}\, H \tag{21}$$

where

$$H^{\mathrm{T}} = \begin{bmatrix} \dfrac{\partial f}{\partial x_i} & \dfrac{\partial f}{\partial x_j} & \dfrac{\partial f}{\partial y_i} & \dfrac{\partial f}{\partial y_j} \end{bmatrix} \tag{22}$$

This leads to

$$\sigma_f^2 = \sigma^2\, \frac{(x_i\, d^2 - x_j)^2 + (x_i\, d^2 - x_j)^2 + (x_i\, d^2 - x_j)^2 + (x_i\, d^2 - x_j)^2}{\xi} \tag{23}$$

Equation (23) can be evaluated using the measurements, which leads to second-order effects only. Results of a typical Monte-Carlo run are shown in Fig. 13. In particular, the top plot uses equation (14), while the bottom plot uses equation (15).

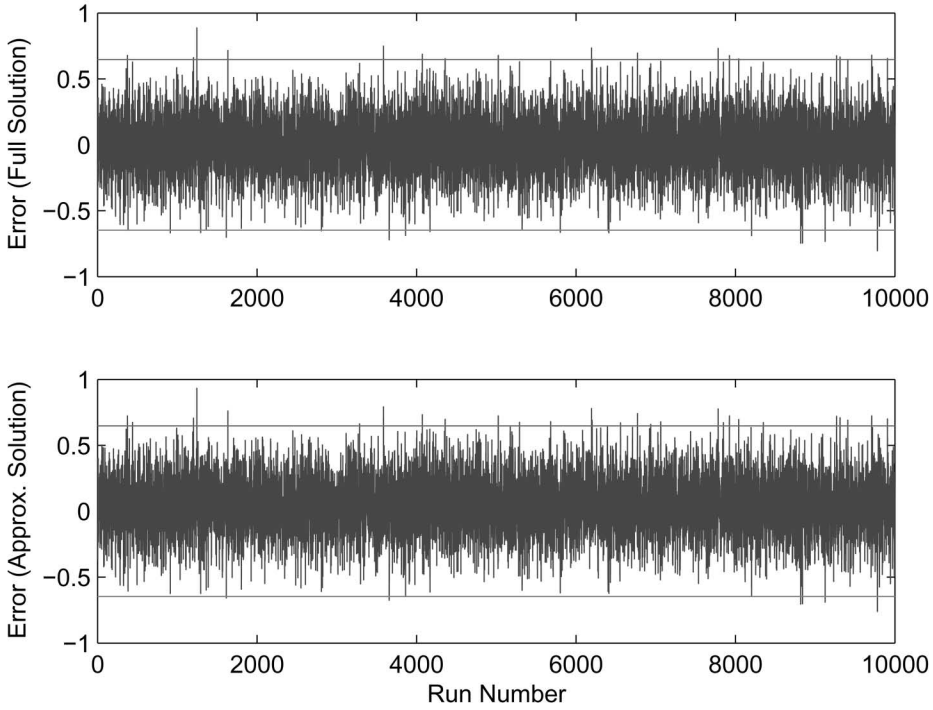

FIG. 13. Errors and 3σ Bounds for a Typical Run.

Conclusion

This paper presents a novel Star-ID method for an uncalibrated star camera, called *Nondimensional Star-ID* algorithm. The proposed method is derived from the fact that the angles of focal plane triangles (formed by the star locations), are weakly dependent on the camera focal length, and on the optical axis offsets. The proposed method is particularly suitable for a poorly calibrated camera, and it can be well adopted as a back-up approach to solve the lost-in-space case of the Star-ID process. Finally, this approach is particularly suitable to make the ground calibration for night-sky experiments easier, as well as the in-flight calibrations.

Acknowledgments

The authors are deeply in debt to two unknown reviewers who greatly improved this paper. In particular, the first reviewer performed an outstanding and extremely detailed review, highlighting both needed conceptual clarifications and editing issues, while the second reviewer provided us with the entire "Error Variance Analysis" section, and included the software code to produce Fig. 13.

References

[1] SAMAAN, M. A., GRIFFITH, T., SINGLA, P., JUNKINS, J. L. "Autonomous On-Orbit Calibration Of Star Trackers," 2001 Core Technologies for Space Systems Conference, Colorado Springs, CO, November 27–30, 2001.

[2] KETCHUM, E. A. and TOLSON, R. H. "Onboard Star Identification Without *a Priori* Attitude Information," *Journal of Guidance, Control, and Dynamics,* Vol. 18, No. 2, March-April 1995, pp. 242–246.

[3] MORTARI, D., JUNKINS, J. L., and SAMAAN, M. A. "Lost-In-Space Pyramid Algorithm for Robust Star Pattern Recognition," presented as paper AAS 01-004 at the Guidance and Control Conference, Breckenridge, Colorado, January 31–February 4, 2001.

[4] MORTARI, D., POLLOCK, T. C., and JUNKINS, J. L. "Towards the Most Accurate Attitude Determination System Using Star Trackers," *Advances in the Astronautical Sciences,* Vol. 99, Pt. II, pp. 839–850.

[5] SHALOM, E., ALEXANDER, J. W., and STANTON, R. H. "Acquistion and Tracking Algorithms for the ASTROS Star Tracker," presented as paper AAS 85-050 at The Annual Rocky Mountain Guidance and Control Conference, Keystone, CO, 1985.

[6] SAMAAN, M. A., MORTARI, D., and JUNKINS, J. L. "Recursive Mode Star Identification Algorithms," presented as paper AAS 01-194 at the Space Flight Mechanics Meeting, Santa Barbara, CA, February 11–14, 2001.

[7] MORTARI, D. "Search-Less Algorithm for Star Pattern Recognition," *The Journal of the Astronautical Sciences,* Vol. 45, No. 2, April-June 1997, pp. 179–194.

[8] URL http://www.fillfactory.com/htm/products/datasheet/star1000.pdf.